

The Feasibility of Interference Alignment over Measured MIMO-OFDM Channels

Omar El Ayach, Steven W. Peters, and Robert W. Heath, Jr.

Wireless Networking and Communications Group

The University of Texas at Austin, Austin, Texas

{omarayach, speters, rheath}@mail.utexas.edu

Abstract

Interference alignment (IA) has been shown to provide all users of an interference channel with half the capacity achievable in an interference free point-to-point link resulting in linear sum capacity scaling with the number of users in the high SNR regime. The linear scaling is achieved by cooperatively precoding transmitted signals to align interference subspaces at the receivers, effectively reducing the number of discernible interferers. The theory of IA was derived under assumptions about the richness of the propagation channel; practical channels do not guarantee such ideal characteristics. This paper presents the first experimental study of IA in measured multiple-input multiple-output orthogonal frequency-division multiplexing (MIMO-OFDM) interference channels. We show that IA achieves the claimed scaling factors in a wide variety of measured channel settings for a 3 user, 2 antennas per node setup. In addition to verifying the claimed performance, we characterize the effect of several realistic system imperfections such as channel estimation error, feedback delay, and channel spatial correlation, on sum rate performance.

I. INTRODUCTION

Interference alignment (IA) is a transmission strategy for the interference channel that results in sum capacities that scale linearly, at high SNR, with the number of users in the system [1]. Interference alignment cooperatively aligns signals over the time, space, or frequency dimensions. In multiple-input multiple-output (MIMO) interference channels, as considered in this paper, IA aligns in the spatial dimension provided by the use of multiple antennas. The key idea of MIMO IA is to construct transmit precoders such that interference aligns at each receiver and spans only a strict subspace of the receive space, thus providing interference free subspaces for the desired signals. To achieve alignment and the maximum gains, however, certain dimensionality constraints need to be satisfied; alignment is only possible for a certain numbers of users if given a sufficient number of transmit and receive antennas.

MIMO interference alignment, as well as alignment in other dimensions, was first studied in [1]–[4]. Since then, IA has been examined further from several angles. After theoretically proving IA’s achievements in terms of sum capacity scaling, a distributed iterative algorithm for constructing MIMO IA precoders in reciprocal channels is suggested in [5]. In [6] an improved algorithm with no reciprocity assumption is suggested. Other solutions exist for symmetric networks [7], cellular networks [8], single-input single-output networks [9], and SISO networks with limited feedback [10]. More recent work, while still theoretical, addresses the feasibility of IA in terms of network structure and channel state information demands [11]–[13]. For example, [11] gives feasibility conditions on the number of antennas needed per node, while [12] examines the possibility of applying IA to a two user network with no channel state information at the transmitter. Extending the IA concept to larger networks, [14] applies IA to large scale Gaussian interference networks to derive new bounds on sum capacity. The work in [5]–[14] has helped better quantify the gains of IA and thus bring it closer to reality; however, practical feasibility is still an open question.

All theoretical results thus far were derived using baseband models with channels drawn independently from a continuous distribution; this represents scattering too rich to be observed in practical system with line-of-sight channels and potentially co-located users. Moreover, there are no comprehensive measurements of the interference channel suitable for studying IA in practice. The only comparable results on multiuser MIMO channel measurements, not directly related to IA, target simpler setups consisting of a single base station and several receivers, and thus do not provide the required data on measured interference channels [15], [16]. Work done in [17], for example, presents multiuser measurements formed by concatenating separate single user measurements, claiming that the static measurement environment ensures validity of the results. Related work on demonstrating IA in practice is limited to [18], which tested a hybrid version of IA coupled with interference cancellation and successive decoding in a single carrier narrowband MIMO wireless local area

network. The work in [18] does not provide insight into the performance of the original MIMO IA solutions in realistic wideband channels and, moreover, downplays the importance of synchronization and other physical layer concepts in the interference channel due to its narrowband nature. Consequently, the viability of IA in measured propagation channels has not been evaluated.

In this paper, we establish the feasibility of MIMO IA in real world propagation channels, with no frequency or time extensions. To acquire suitable channel measurements, we implemented a MIMO-OFDM measurement testbed for the 3-user 2×2 MIMO interference channel, using a software defined radio platform [19]. We gave special attention to the proper implementation of a synchronized MIMO-OFDM physical layer to guarantee the validity of our measurements; a consideration that was not emphasized in previous work [15]–[18]. We augment the system we implemented in [19] to accommodate measurement setups over large outdoor areas and perform channel measurements for a variety of indoor and outdoor static node deployments and therefore extend the preliminary indoor results derived in [19]¹. We summarize the data collected and use it to establish the true feasibility of IA in measured wideband channels. We examine the average sum rate achieved versus signal-to-noise ratio and show that, as predicted in theory, IA outperforms time division multiple access (TDMA), considered in [19], as well as other MIMO techniques, and achieves the maximum degrees of freedom in our setup. Finally, we elaborate and comment on a variety of overlooked system and channel imperfections, such as spatial correlation, collinearity, feedback delay, estimation error, and their effect on the performance of IA which were kept as open questions in [19].

Throughout this paper we use the following notation: \mathbf{A} is a matrix, and a is a scalar; \mathbf{A}^* denotes the conjugate transpose of \mathbf{A} , and $\|\mathbf{A}\|_F$ is the Frobenius norm of \mathbf{A} ; $\text{trace}(\mathbf{A})$ is the trace of \mathbf{A} ; \mathbb{C}^N is the N -dimensional complex space. Other notation is defined as needed.

This paper is organized as follows. Section II briefly presents the MIMO-OFDM signal model in the presence of interference, Section III summarizes the basic idea of IA and introduces several IA solutions as well as algorithms used for comparison. Section IV details both the hardware and software used in our measurement testbed. Sections V and VI present and discuss the measurements obtained from our setup in indoor and outdoor environments respectively. We also analyze the performance of IA over measured channels and characterize the effects of practical system and channel imperfections in Section VII. We conclude with Section VIII

II. MIMO INTERFERENCE SIGNAL MODEL

Consider the general K -user narrowband interference channel shown in Figure 1 with M_k transmit antennas at transmitter k and N_m receive antennas at receiver m . In the interference channel studied, each transmit node

¹We also obtain larger data sets, in more indoor and outdoor antenna and node configurations. The performance analysis is also extended to include various other interference channel algorithms. We also characterize the effect of several practical system and channel impairments.

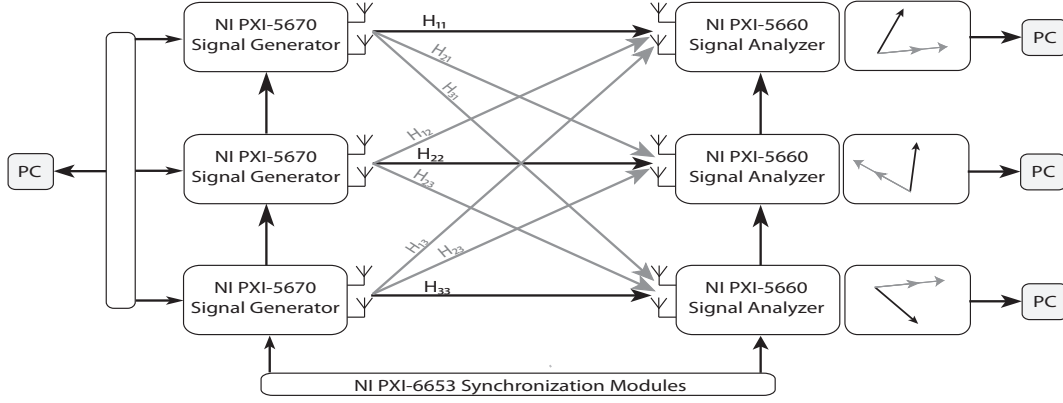


Fig. 1. Simplified hardware block diagram.

k communicates with its corresponding designated receiver k and interferes with all other receivers, $m \neq k$, sharing the medium. In this section we explain the MIMO interference signal model in the general case, though in the remainder of this paper we specialize to the $K = 3$ user 2×2 interference channel.

The received signal at node k , in the absence of timing and frequency offset impairments, is given by

$$\mathbf{y}_k = \mathbf{H}_{k,k} \mathbf{F}_k \mathbf{s}_k + \sum_{m \neq k} \mathbf{H}_{k,m} \mathbf{F}_m \mathbf{s}_m + \mathbf{v}_k, \quad (1)$$

where \mathbf{y}_k is the $N_k \times 1$ received signal vector, $\mathbf{H}_{k,m}$ is the $N_k \times M_m$ normalized channel matrix from transmitter m to receiver k with elements drawn from an arbitrary i.i.d. continuous distribution, \mathbf{F}_k is the precoding matrix used at node k , \mathbf{s}_k is the transmitted QAM or PSK symbol at node k , and \mathbf{v}_k is a complex vector of i.i.d. circularly symmetric white Gaussian noise with covariance matrix $\mathbb{E}[\mathbf{v}_k \mathbf{v}_k^*] = \sigma^2 \mathbf{I} \forall k$. Note that in this model, for simplicity, the transmit power is assumed to be 1, and the effects of large scale fading are neglected.

Since the capacity region of the interference channel, formed by many rate constraints, remains unknown, the performance of IA can not be compared to a capacity achieving scheme. We, therefore, evaluate the performance of IA by studying the achieved sum rate, one of the faces of the capacity region, and, more importantly, a metric that defines the total throughput of the network. The sum rate is calculated as

$$C = \sum_{k=1}^K \log_2 \left| \mathbf{I} + (\sigma^2 \mathbf{I} + \mathbf{R}_k)^{-1} (\mathbf{H}_{k,k} \mathbf{F}_k \mathbf{F}_k^* \mathbf{H}_{k,k}^*) \right|, \quad (2)$$

where

$$\mathbf{R}_k = \sum_{m \neq k} \mathbf{H}_{k,m} \mathbf{F}_m \mathbf{F}_m^* \mathbf{H}_{k,m}^*,$$

is the interference covariance matrix and SNR is reflected, in simulation, by varying the noise power while keeping the normalized channels constant.

MIMO can be combined with Orthogonal Frequency Division Multiplexing (OFDM) to transform wideband frequency selective channels into a collection of frequency flat subchannels [20]. OFDM allows the system to treat a single wideband channels as many parallel, i.e. non-interfering, frequency flat subchannels. The resulting MIMO-OFDM transmission technique for broadband channels is now widely deployed in commercial wireless systems such as IEEE 802.11n and 802.16a and has been demonstrated to improve performance of wireless networks [21]. When considering a MIMO-OFDM frequency selective and sufficiently slow-fading channel with N subcarriers, the received signal at node k for subcarrier n at the input of the signal decoder is given by

$$\mathbf{y}_k[n] = \mathbf{H}_{k,k}[n]\mathbf{F}_k[n]\mathbf{s}_k[n] + \sum_{m \neq k} \mathbf{H}_{k,m}[n]\mathbf{F}_m[n]\mathbf{s}_m[n] + \mathbf{v}_k[n], \quad (3)$$

where we use the same notation as in the narrowband system model. In this signal model, we assume perfect carrier recovery and symbol timing estimation at the output of our synchronization modules. We also assume that the impulse response of the channel is shorter than the cyclic prefix used, which guarantees that the wideband channel decouples into a collection of parallel frequency flat channels, thus allowing us to write the received signal as in (3).

Under the assumptions of perfect timing and carrier recovery, and the decoupling of the wideband channel into parallel subchannels, we study performance using the sum rate of the system. The sum rate in bits/s/Hz can be derived by averaging the rate achieved in a narrowband MIMO precoding system over the channels observed on each of the subcarriers. This is analogous to the expression derived in [22] to study the ergodic capacity of a single user MIMO-OFDM channel. The sum rate is, therefore, calculated as

$$C = \frac{1}{N} \sum_{n=1}^N \sum_{k=1}^K \log_2 \left| \mathbf{I} + (\sigma^2 \mathbf{I} + \mathbf{R}_k[n])^{-1} (\mathbf{H}_{kk}[n]\mathbf{F}_k[n]\mathbf{F}_k^*[n]\mathbf{H}_{kk}^*[n]) \right|, \quad (4)$$

where

$$\mathbf{R}_k[n] = \sum_{m \neq k} \mathbf{H}_{k,m}[n]\mathbf{F}_m[n]\mathbf{F}_m^*[n]\mathbf{H}_{k,m}^*[n]$$

is the per-subcarrier interference covariance matrix.

III. INTERFERENCE ALIGNMENT AND OTHER TRANSMIT TECHNIQUES

In this section we summarize several algorithms for dealing with interference. The algorithms are run on the measured channel data to demonstrate the expected performance in practice. We start with the closed-form solution for interference alignment, which is valid only for the three user system model. Then we summarize iterative interference alignment and a signal-to-interference-plus-noise (SINR) maximizing solution. We also review the algorithms, which we evaluate interference alignment's performance against. We review TDMA, random beamforming, SVD beamforming that chooses precoders to transmit signals in the dominant eigenspace

of the channel, and greedy interference avoidance that accounts for the received interference and attempts to maximize SINR. While IA, which chooses precoders for perfect alignment, and its variants are optimal in terms of sum rate scaling, and while SINR maximization improves IA in the low SNR regime by choosing precoders with consideration to post-alignment SNR, none of these strategies is proven to be the capacity achieving solution.

A. Closed Form Interference Alignment

IA, using an adequate number of antennas per node, aims at choosing the precoding matrices $\{\mathbf{F}_k\}$ to force the received interference at each of the K receivers to lie within a lower dimensional subspace. Specifically, if receiver k intends on decoding S_k independent data streams with no interference, it must restrict interference to a $N_k - S_k$ dimensional subspace of the receive signal space, \mathbb{C}^{N_k} . After alignment, the receiver decodes its S_k streams by projecting on the S_k dimensional subspace orthogonal to the aligned interference.

Stated more formally, let $\mathbf{W}_k[n]$ be the $N_k \times S_k$ matrix describing the orthonormal basis for the interference free subspace used at node k and subcarrier n . To decode, node k first projects on the basis of the interference free subspace. Ignoring the AWGN noise term, this yields

$$\mathbf{W}_k[n]^* \mathbf{y}_k[n] = \mathbf{W}_k[n]^* \left(\mathbf{H}_{k,k}[n] \mathbf{F}_k[n] \mathbf{s}_k[n] + \sum_{m \neq k} \mathbf{H}_{k,m}[n] \mathbf{F}_m[n] \mathbf{s}_m[n] \right). \quad (5)$$

For perfect interference alignment, the received interference must therefore lie in the nullspace of $\mathbf{W}_k[n]^*$, which gives

$$\mathbf{W}_k[n]^* \mathbf{H}_{k,m}[n] \mathbf{F}_m[n] \mathbf{s}_m[n] = \mathbf{0}, \quad \forall m \neq k \quad (6)$$

Effectively, this restricts all interference to the chosen $N_k - S_k$ dimensional nullspace, thus satisfying

$$\text{span}(\mathbf{H}_{k,m}[n] \mathbf{F}_m[n]) \subseteq \text{null}(\mathbf{W}_k[n]^*), \quad \forall m \neq k, \quad (7)$$

where $\text{span}(\mathbf{A})$ denotes the space spanned by the column vectors of \mathbf{A} , and $\text{null}(\mathbf{A})$ denotes the space spanned by all vectors \mathbf{x} such that $\mathbf{A}\mathbf{x} = \mathbf{0}$. In addition to satisfying (6), the interference alignment solution must satisfy

$$\text{rank}(\mathbf{W}_k[n]^* \mathbf{H}_{k,k}[n] \mathbf{F}_k[n]) = S_k \quad (8)$$

to successfully decode all S_k streams.

This spatial alignment approach, with possible symbol extensions, guarantees the maximum number of degrees of freedom as shown by [1] and is optimal in the high SNR regime. Interference alignment does not claim optimality at low-to-moderate SNR where the optimal multiple access strategy is still unknown. Our work focuses on the three 2×2 user case, proven to provide each user with one interference free spatial stream. Although closed form interference alignment solutions do not yet exist for networks with more than three users,

we test the performance of the existing 3 user solution presented in [1]. In the 3 user case, the conditions for interference alignment presented in (6), (7), and (8) can be satisfied by choosing the precoding matrices as

$$\mathbf{F}_1[n] = \text{eig} \left((\mathbf{H}_{3,1}[n])^{-1} \mathbf{H}_{3,2}[n] (\mathbf{H}_{1,2}[n])^{-1} \mathbf{H}_{1,3}[n] (\mathbf{H}_{2,3}[n])^{-1} \mathbf{H}_{2,1}[n] \right), \quad (9)$$

$$\mathbf{F}_2[n] = (\mathbf{H}_{3,2}[n])^{-1} \mathbf{H}_{3,1}[n] \mathbf{F}_1[n], \quad (10)$$

$$\mathbf{F}_3[n] = (\mathbf{H}_{2,3}[n])^{-1} \mathbf{H}_{2,1}[n] \mathbf{F}_1[n], \quad (11)$$

where $\text{eig}(\mathbf{H})$ is the eigenvector corresponding to the largest eigenvalue of \mathbf{H} .

It is important to note that the solution presented in (9), (10), and (11) is not unique. To illustrate this point in the presented closed form solution, one can start by setting $\mathbf{F}_2[n]$ or $\mathbf{F}_3[n]$ and defining $\mathbf{F}_1[n]$ accordingly, thus yielding a different alignment solution. Though all these rotationally invariant solutions align interference at the receivers, they may have significantly different performance, and thus to truly maximize the achievable sum rate one must choose the best out of the set of solutions. The exact number of solutions to this system is still unknown, and an efficient method to determine the globally optimum one, in terms of sum rate, is yet to be found.

B. Iterative Interference Alignment

In [6], alignment in a K -user network is formulated in a general alternating minimization framework. The alternation happens between the K precoders and the K interference subspaces. This problem is then solved via iterative alternating minimization. The alignment problem is viewed as minimizing the “leakage” interference power over the set of precoders and interference subspaces

$$\min_{\substack{\mathbf{F}_m[n]^* \mathbf{F}_m[n] = \mathbf{I}, \forall m \\ \mathbf{C}_k[n]^* \mathbf{C}_k[n] = \mathbf{I}, \forall k}} \sum_{k=1}^K \sum_{\substack{m=1 \\ m \neq k}}^K \|\mathbf{H}_{k,m}[n] \mathbf{F}_m[n] - \mathbf{C}_k[n] \mathbf{C}_k[n]^* \mathbf{H}_{k,m}[n] \mathbf{F}_m[n]\|_F^2, \quad (12)$$

which can be solved for $\mathbf{F}_m[n]$ by keeping $\mathbf{C}_k[n]$ fixed, and vice versa. As a result, the pseudo code for such a minimization is

- 1) Choose the set $\{\mathbf{F}_m[n]\}$ randomly.
- 2) Choose the columns of $\mathbf{C}_k[n]$ to be the $N_k - S_k$ dominant eigenvectors of $\sum_{m \neq k} \mathbf{H}_{k,m}[n] \mathbf{F}_m[n] \mathbf{F}_m[n]^* \mathbf{H}_{k,m}[n]^* \forall k$.
- 3) Choose the columns of $\mathbf{F}_m[n]$ to be the S_m least dominant eigenvectors of $\sum_{k \neq m} \mathbf{H}_{k,m}[n]^* (\mathbf{I}_{N_k} - \mathbf{C}_k[n] \mathbf{C}_k[n]^*) \mathbf{H}_{k,m}[n] \forall m$.

4) Repeat steps 2 and 3 until convergence.

where the linear receivers could then be $\mathbf{W}_k[n] = \mathbf{I}_{N_k} - \mathbf{C}_k[n]\mathbf{C}_k[n]^*$.

Convergence in the algorithm is guaranteed by the fact that steps 2 and 3 can only decrease the non-negative objective function. The non-convex nature of the objective function, however, implies the presence of multiple local optima to which the algorithm can converge, and thus convergence to the global optimum is not guaranteed. Further, recall that interference alignment does not necessarily maximize the sum capacity in (2). Therefore, to increase the sum rate, this iterative algorithm (and the others we discuss) can be improved by performing several random initializations and choosing the one that results in the largest performance metric. Choosing the best out of multiple randomly generated initial conditions is demonstrated in Section VI.

C. Maximum SINR Algorithm

Interference alignment does not target maximizing sum capacity directly. One particular limitation is that it focuses on making the signal-to-interference ratio infinite; it does not attack more relevant performance measures like the post-processing signal-to-interference-plus-noise ratio. As a result, perfect alignment often comes at the cost of lower post-alignment SINR, or effectively sum rate, the metric we are actually interested in maximizing. We can thus consider an improved adaptation of iterative IA that maximizes other metrics, perhaps without aligning interference perfectly. One such improvement maximizes the total SINR of the network, given by

$$S(\mathbf{F}_1[n], \mathbf{F}_2[n], \dots, \mathbf{F}_K[n]) = \frac{\sum_{k=1}^K \|\mathbf{W}_k[n]\mathbf{H}_{kk}[n]\mathbf{F}_k[n]\|_F^2}{\sum_{k=1}^K \left(\sum_{m \neq k} \|\mathbf{W}_k[n]\mathbf{H}_{k,m}[n]\mathbf{F}_m[n]\|_F^2 + \text{trace}(\mathbf{W}_k[n]\mathbf{Q}_k[n]\mathbf{W}_k[n]^*) \right)}, \quad (13)$$

where $\mathbf{Q}_k[n]$ is the noise covariance matrix at receiver k and subcarrier n and $\mathbf{W}_k[n]$ is now the combiner used at receiver k [23].

Instead of optimizing the sum capacity or the sum SINR (both which are not quite tractable), this algorithm optimizes the sum signal power over the sum interference-plus-noise power which is a relatively easier task. Since the $\mathbf{F}_k[n]$ and $\mathbf{W}_k[n]$ are not independent, a closed-form solution for this objective function is unlikely, however, we can solve it via an alternating minimization. For tractability, the precoders are constrained to have columns of equal norm, thus satisfying $\mathbf{F}_k^* \mathbf{F}_k = \frac{1}{S_k} \mathbf{I}, \forall k$ [23]. By fixing all \mathbf{F}_m we can solve for \mathbf{W}_k as

$$\mathbf{W}_k[n] = \text{eig} \left(\left(\sum_{m \neq k} \mathbf{H}_{k,m}[n]\mathbf{F}_m[n]\mathbf{F}_m[n]^* \mathbf{H}_{k,m}[n]^* + \mathbf{R}_k[n] \right)^{-1} \mathbf{H}_{kk}[n]\mathbf{F}_k[n]\mathbf{F}_k[n]^* \mathbf{H}_{kk}[n]^* \right), \quad (14)$$

Conversely, by fixing all $\mathbf{W}_k[n]$, we can solve for the precoders as

$$\mathbf{F}_m[n] = \text{eig} \left(\left(\sum_{k \neq m} \mathbf{H}_{k,m}[n]^* \mathbf{W}_k[n]^* \mathbf{W}_k[n] \mathbf{H}_{k,m}[n] \right)^{-1} \mathbf{H}_{m,m}[n]^* \mathbf{W}_m[n]^* \mathbf{W}_m[n] \mathbf{H}_{m,m}[n] \right). \quad (15)$$

Note that in the 3-user 2×2 channel case considered in this paper, we are limited to one stream per user but the results can be generalized to any number of achievable streams [5]. This results in an algorithm pseudo-code given by

- 1) Choose the set $\{\mathbf{F}_m[n]\}$ randomly.
- 2) Choose the columns of $\mathbf{W}_k[n]$ as given by (14).
- 3) Choose the columns of $\mathbf{F}_m[n]$ as given by (15).
- 4) Repeat steps 2 and 3 until convergence.

Again, this algorithm will benefit from picking the best result out of a set of random initializations and will achieve consistently higher sum rates at all SNR levels. For multiple streams this must be solved for each column of each matrix, resulting in non-orthogonal solutions.

D. Other Transmit Strategies

In this paper we consider the versions of interference alignment present in sections III-A, III-B, and III-C and compare performance to earlier transmit techniques typically used in interference networks. In this section we briefly present the transmission techniques used for performance evaluation.

In a network employing TDMA, transmissions from different users are orthogonal in time, meaning that only one user transmits in any given time slot. In this system, users transmit in a round robin fashion. TDMA systems can take advantage of multiuser diversity by selecting, in every time slot, the user with the most favorable channel, in terms of capacity, to transmit in that time slot. This requires channel information to be known at the transmitter, to make the selection process possible, and thus is a more fair comparison to IA which also requires this knowledge. Note that TDMA is conceptually equivalent to other orthogonal resource allocation techniques such as FDMA, where orthogonality is in the frequency domain.

We also consider several variations of beamforming, namely random, SVD, and greedy interference avoidance. Random beamforming, as the name suggests, chooses the beamforming vectors $\{\mathbf{F}_k\}$ to be random, non-orthogonal, Gaussian vectors, i.e. $\mathbf{F}_k \sim \mathcal{CN}(\mathbf{0}, \mathbf{I})$ which are later normalized. SVD beamforming, or dominant eigenmode transmission [24] chooses beamforming vectors as $\mathbf{F}_k = \text{eig}(\mathbf{H}_{kk})$ and neglects the interference covariance matrix. Choosing the channel's most dominant eigenvector for transmission ensures that the signal is multiplied by a factor equal to the largest eigenvalue of the channel, thus maximizing SNR at the receiver but not the SINR. In the presence of interference, as in equation (3), the rate achieved by each user depends on the matrix $(\sigma^2 \mathbf{I} + \mathbf{R}_k[n])^{-1/2} (\mathbf{H}_{kk}[n])$. The greedy interference avoidance approach, which we also consider for comparison, aligns its signal along the most dominant eigenmode of this matrix, thus sending in the direction it receives the least interference in [25]. Since the choice of a user's precoder using the greedy interference avoidance approach affects the interference subspaces observed in the network, this precoder selection is done

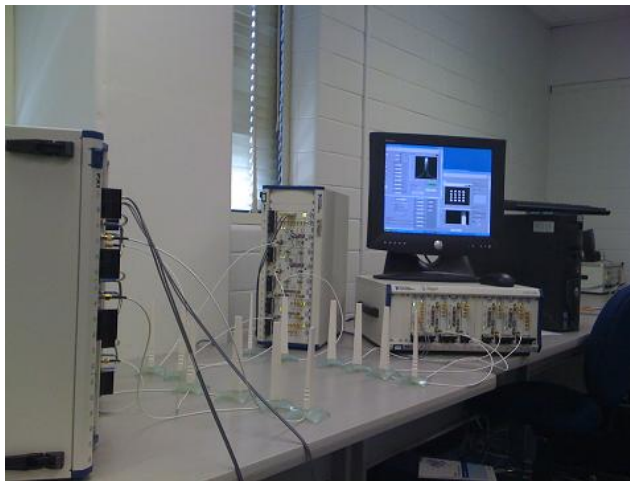


Fig. 2. Picture of the measurement testbed implemented showing the antennas, RF front end equipment, as well as a sample of the software interface.

for many iterations, in hope of reaching a fixed point, but the algorithm does not always converge [26].

IV. SYSTEM IMPLEMENTATION AND MEASUREMENT SETUP

In this section we present the main software and hardware details of the measurement testbed developed at UT Austin. We discuss the main concepts in our MIMO-OFDM system implementation such as training, channel estimation, and carrier recovery. We also introduce the system parameters used in our experiments to collect channel measurements.

A. Software Implementation

Our MIMO-OFDM testbed software, implemented in LabVIEW, uses the parameter values indicated in Table I for all communicating users in the network. We use OFDM modulation with an FFT size of 256 and a 64 sample guard interval. The total signal bandwidth used in our measurement setup is 16 MHz, which results in an effective OFDM symbol time of $20\mu s$. Communication is done at a carrier frequency ranging from 2GHz to 2.7GHz with most measurements done in the 2.4GHz industrial, scientific, and medical (ISM) band. Data on each subcarrier can be modulated using BPSK or M-QAM.

We use periodic frequency domain pilot symbols for each user to estimate the channel and equalize received data [20]. Training for each user is sent sequentially, i.e. orthogonal in time, and in each training phase, pilot symbols are shared among transmit antennas as shown in Figure 3, i.e subcarriers are divided among transmit antennas to achieve orthogonal training for each antenna [27]. To obtain a full frequency response for each antenna, we transmit pilot symbols in pairs, with opposite subcarrier multiplexing. Assuming perfect time and frequency synchronization at the output of the synchronization software blocks, and assuming that all

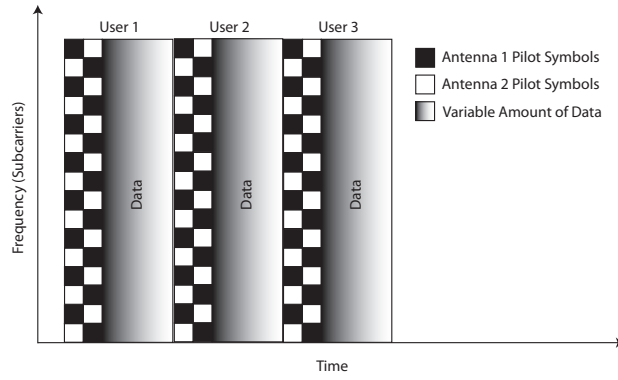


Fig. 3. Simplified pilot and data example for measurement.

training sequences are known to all users, with all antennas sending sufficiently cyclically prefixed training data, orthogonal in time or frequency, we estimate the channel using least-squares frequency domain estimation and apply a frequency domain zero forcing equalizer to any sent data, a common method similar to narrowband equalization [28].

The ratio of pilot-to-data symbols is variable. This variable ratio can be used to accommodate channels with short coherence times and can emulate channel estimation frequencies used in emerging MIMO wireless standards. To provide extensive channel measurements, we send 2 pilot symbols for every OFDM data symbol. This effectively sends pilot symbols from all users in the system, with minimal data in between as shown in Figure 3, thus keeping the measurement time in the microsecond range. Sending data in the measurement exercise is recommended to verify correct reception and decoding, thus ensuring that the recorded channel measurements correspond to successful transmissions.

Pilot symbols are used to estimate frequency offsets between each transmit-receive pair as well. For proper MIMO communication, transmit chains corresponding to the 2 transmit antennas per user are synchronized to justify the assumption of a single frequency offset per transmit-receive pair. For the sake of our channel measurements, however, and since we want to test the performance of IA in the absence of such impairments, we synchronize all users' transmit chains. Our measurements show that the use of the onboard high precision oscillators to synchronize all transmit RF chains results in frequency offsets within a 100Hz of each other which are estimated and further corrected in software via MIMO-OFDM synchronization techniques presented in [29]. Software correction is done in stages starting with a coarse time synchronization, fractional frequency offset estimation, integral frequency offset estimation and finally fine time synchronization [29]. The details of the hardware clock will be given when discussing the hardware setup.

TABLE I
MIMO-OFDM SYSTEM PARAMETERS

Carrier Freq.	2.4GHz
Transmit Power	6 dBm
Bandwidth	16MHz
FFT Size	256
Subcarrier Spacing	6.25kHz
Guard Interval	64 samples
Total Symbol Duration	20 μ s
MIMO Scheme	Alamouti

B. Hardware Description

Our hardware setup consists of four NI PXI-1045 chassis connected to 3 PCs [30]. The first PC controls 2 PXI chassis, containing the three users' transmit chains, and one user's receive chains. The remaining two PXI-1045 chassis house the receive chains of the remaining two users and are each connected to a separate PC. In addition to the RF hardware installed, each PXI-1045 chassis holds a NI PXI-6653 module for timing and synchronization. A simplified hardware block diagram is shown in Figure 1.

Each transmitter, or RF signal generator, named PXI-5670, consists of two physical units, an arbitrary waveform generator, NI PXI-5421, and an upconverter, NI PXI-5610 [31]. The arbitrary waveform generator produces an intermediate frequency signal which is later modulated to RF via the upconverter. Each receiver, or RF signal analyzer, named NI PXI-5660, constitutes a downconverter, NI PXI-5600, and a digitizer, NI PXI-5620 [32]. On the receive side, the downconverter downconverts the signal to an intermediate frequency after which the digitizer takes over and samples the waveform which is then sent to the PC for processing using the LabView software blocks. Note that each user consists of two transmit and two receive chains, totaling six transmit chains and six receive chains for our overall network setup.

This RF setup is not entirely new, and has been used in papers such as [33] to implement single user MIMO communication. Our setup, however, is significantly more complex to support multiple users whose hardware components are housed in different chassis and controlled by different PCs. Moreover, software implementation differs greatly in the methods used for training and channel estimation as well as carrier recovery. The software and hardware has been significantly augmented to support proper concurrent transmission for all users in the network.

To support the cross chassis synchronization needed for this multi-user prototype, we install NI PXI-6653 timing and synchronization modules in each PXI-1045 chassis [34]. This module has a high stability reference

oven-controlled-crystal-oscillator (OCXO) which can be exported to other chassis via an external PFI connector, thus enabling synchronization. Locking all the transmitters' phase locked loops to this high precision OCXO ensures a unique carrier frequency offset at each receiver for all transmitters. Although frequency offset correction is implemented in software, this synchronization further strengthens the validity of the obtained measurements. Our measurements indicate that the difference in frequency offsets between transmitters, when locked into the reference signal from the PXI-6653, is below 100 Hz at a carrier of 2.4 GHz. This remaining frequency offset is then estimated and corrected in software [29].

In addition to synchronizing clocks, the PXI-6653 allows us to export the trigger generated when the master user begins signal generation. This digital signal is then used to trigger generation at the other transmitters. While digitally triggered acquisition was possible in small-scale indoor setups such as those presented in [19], our outdoor measurement setup stretches over distances of about 250ft, making digital triggering impossible. To accommodate outdoor setups, acquisition is triggered via analog edge triggers. Under this type of triggering, the receiver starts recording samples whenever the received signal level exceeds a predefined threshold. We discard any measurement that has been corrupted by the ambient interference in the 2.4 GHz ISM band and thus retain only valid interference free measurements.

This triggered acquisition and clock synchronization ensure that our measurements include only channel effects, and are thus free of any timing impairments. The use of digital triggers also uniformizes the acquisition process over all receivers and thus guarantees that all receivers process the same symbols, without missing transmissions done while processing previous data.

V. INDOOR RESULTS

In this Section we present some of the results collected using our measurement setup. We then use the collected measurements to evaluate the performance gains of using interference alignment.

We conduct experiments in the Wireless Laboratory, shown in Figure 4, in the Engineering Science Building room 113 at The University of Texas at Austin. Transmitters and receivers are placed at varying distances, ranging from 1 meter, to approximately 6 meters apart, both of which for a wavelength of 12.5cm are well in the far field of the other node's antennas [35], in both line-of-sight and non-line-of-sight arrangements. The measurement campaign details are summarized in Table II. Figure 5 is an example frequency plot of $\|\mathbf{H}_{11}\|$, over 25 packet transmissions to visualize the temporal evolution of the channel. Figure 5 shows limited frequency selectivity as it was generated using a strict line-of-sight arrangement. Also, inspecting Figure 5 reveals that the observed channel variation over successive packet transmissions is minimal. In fact, our measurements indicate that the channel correlation after 200ms remains above 97%.

We then perform experiments in various configurations to systematically study the performance of interference

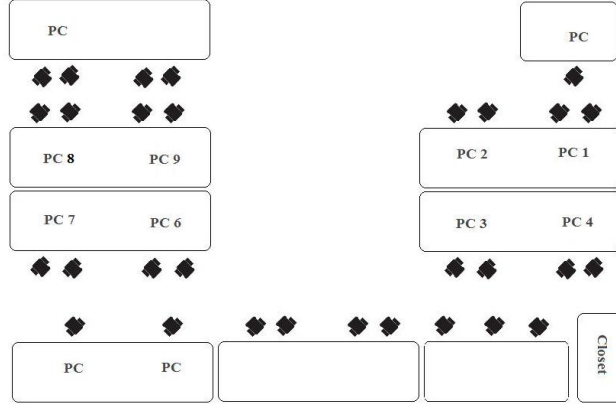


Fig. 4. Schematic of our indoor measurement environment in the Engineering Science building at The University of Texas at Austin. For our indoor measurements, antennas were arranged in various static configurations in this room. Note that not only are the nodes placed at fixed positions, but all objects in this room remain in their fixed locations throughout the duration of the measurement campaign. Indoor measurement details are summarized in Table II.

alignment in realistic node arrangements. The considered configurations facilitate studying the effect of the channel's spatial correlation on performance and feasibility. Interference alignment bases its logic on the fact that (6) and (8) can be simultaneously satisfied, almost surely, when all the elements of the channel matrices are drawn independently at random from a continuous distribution. This independence assumption, however, is not likely to be satisfied in practice. Node deployments might exhibit varying degrees of channel spatial correlation, in which the independent channel assumption does not hold. This possibly hinders the performance of interference alignment. In fact, feasibility, in general, remains an open problem, in the sense that it is still unknown whether one can usually find a set of precoders, $\{\mathbf{F}_k\}$, and combiners, $\{\mathbf{W}_k\}$, that in reality achieve a theoretically achievable degree of freedom allocation in the network. Our measurement results, therefore, give insight into the actual feasibility and performance of this theoretically optimal transmit strategy in realistic channels with actual complexities that are never entirely captured in simulations and models.

To systematically study performance, we arrange antennas a configuration similar to Figure 1 in which all antennas are placed a distance d apart. We conduct measurements for variable values of $d \in \{\lambda/2, \lambda, 2\lambda, 3\lambda, 4\lambda, 5\lambda\}$ to properly study the effect of spatial correlation. The channel's spatial correlation, calculated according to the Kronecker model, is given by

$$\mathbf{R}_{RX} = \frac{1}{\|\Omega\|} \sum_{\Omega} \mathbf{H} \mathbf{H}^*, \quad (16)$$

$$\mathbf{R}_{TX} = \frac{1}{\|\Omega\|} \sum_{\Omega} \mathbf{H}^* \mathbf{H}, \quad (17)$$

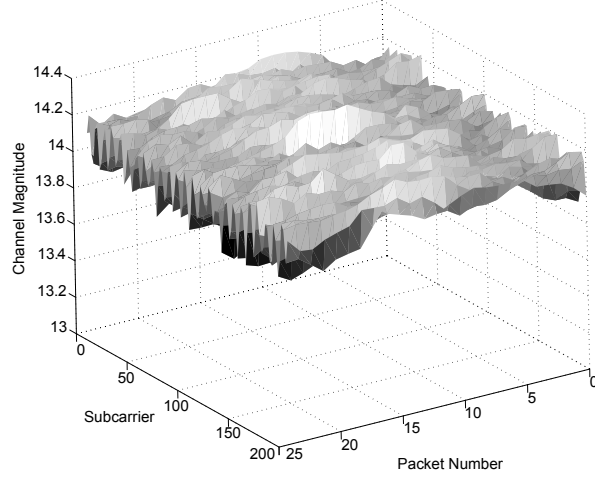


Fig. 5. The temporal evolution of \mathbf{H}_{21} in our static indoor environment. \mathbf{H}_{21} exhibits very limited time selectivity due to the static placement of the nodes and limited motion in the environment.

TABLE II
INDOOR MEASUREMENT DETAILS

Tx-Rx Spacing	$\sim 6m$
Antenna Spacing	$d \in \{0.5\lambda, 1\lambda, 2\lambda, \dots, 5\lambda\}$
Configurations	1. Equidistant nodes & antennas 2. Triangle configuration
# of Measurements	50 for each configuration & antenna spacing
Measurement Duration	$225\mu s$
Time Between Measurements	$\sim 45s$
Receive SNR	$\sim 20dB$
Mobility	Fixed nodes & environment

where Ω is the set of all measurements taken in the considered configuration. When calculating correlation, the channel matrices \mathbf{H} are individually normalized, in this case, to have unit Frobenius norm, $\mathbf{H}/\|\mathbf{H}\|_F$. The norm of the off-diagonal elements of the correlation matrices calculated in equations (16) and (17) for the configuration in Figure 1 is shown in Figure 6. We also conduct measurements with co-located transmitters and receivers on the vertices of a triangle. In this last arrangement, we position transmit-receive pairs at a distance $1m$ apart, and place antennas of the same node once at a distance of $\lambda/2$, yielding a receive correlation of 0.135, and then at 3λ , resulting in a receive correlation of 0.017.

We use the measurements collected to study the performance of interference alignment over the observed channels. Before evaluating IA over real channels, and gauging its performance against previous simulated

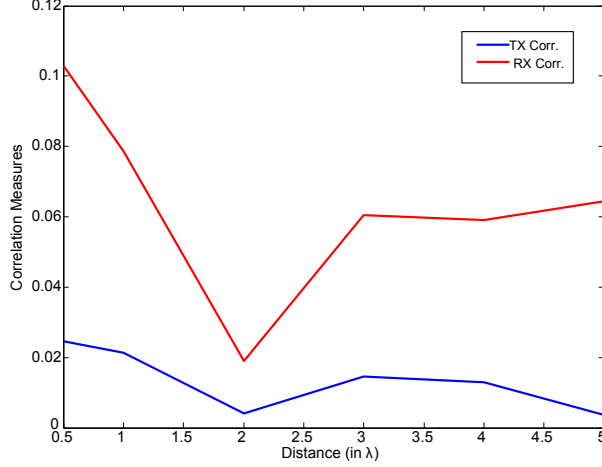


Fig. 6. Channel's Spatial Correlation Vs. Antenna Spacing in the indoor wireless environment averaged over all 3 users.

results, we first obtain normalized channel matrices, $\tilde{\mathbf{H}}$, for fair comparison with the Rayleigh channels generated to have matrix elements of unit variance. We, therefore, normalize the measured channels over the full data set, i.e no time windowing is applied resulting in an effective averaging window equal to the full data set. The normalized channel matrices as shown in equation (18) thus have elements of unit variance, translating into an average Frobenius norm of 2,

$$\tilde{\mathbf{H}}_{k,m} = 2 \frac{\mathbf{H}_{k,m}}{\sqrt{\frac{1}{\|\Omega\|} \sum_{\Omega} \|\mathbf{H}_{k,m}\|_F^2}}, \quad (18)$$

where Ω is the set of all measurements collected in the scenario considered, i.e. when normalizing a matrix obtained when $d = 1\lambda$, Ω would be the set of all channel measurements obtained in that configuration (in our measurements $\|\Omega\| = 50$ as indicated in Table II) [36].

We are primarily interested in verifying the theoretical achievements of the proposed solution in terms of its ability to provide the maximum achievable degrees of freedom in the K -User interference channel, thus allowing systems to approach the capacity of such wireless channels with arbitrarily small gaps at high SNR. By doing so, we will have verified the optimality of interference alignment in the high SNR regime. To that end, Figure 7 plots the ergodic sum rate achieved in our 3-user network setup using (4) for IA and TDMA. For fairness throughout this paper, we compare using TDMA with multiuser diversity, meaning that instead of nodes transmitting in a round robin fashion, in every time slot the user with the most favorable channel, in terms of capacity, is chosen to transmit. Our measurements and simulations indicate, however, that exploiting multiuser diversity in a 3-user network of 2×2 links only achieves sum rate by about 1.5 bits/s/Hz.

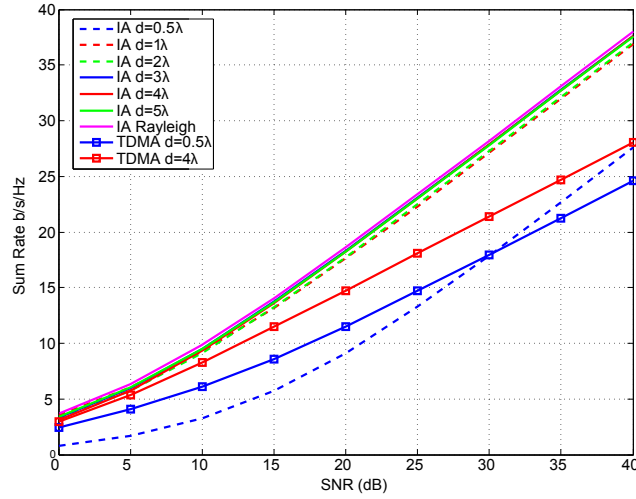


Fig. 7. Network sum rate vs. SNR for the configuration in Figure 1 with several antenna spacings. This confirms that IA outperforms TDMA and achieves the predicted 3 degrees of freedom for this 3 user network.

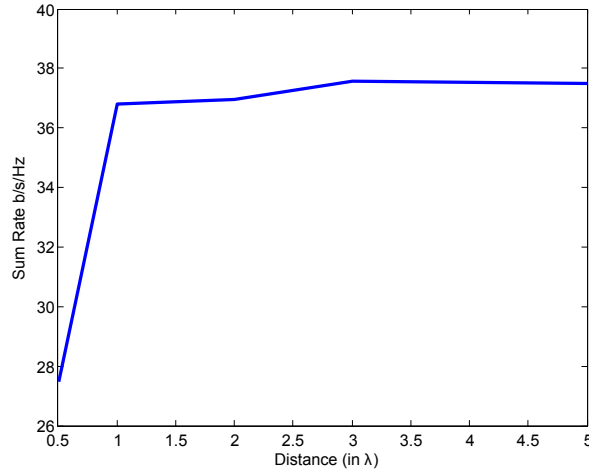


Fig. 8. The network sum rate for the configuration in Figure 1 plotted versus antenna spacing d showing that IA benefits from increased antenna spacing.

As anticipated from theoretical results, Figure 7 verifies the fact that interference alignment outperforms time division multiple access (TDMA), and its equivalent resource allocation schemes. Moreover, we note that the throughput gain observed when using interference alignment is most pronounced in the high SNR regime; which is the case of claimed optimality. Comparing the rate at which network throughput increases with SNR, we observe that interference alignment benefits more from marginal increase of SNR, thus achieves more degrees of freedom than TDMA and its equivalents. The slope of the plots relative to $\log_2(SNR)$ can

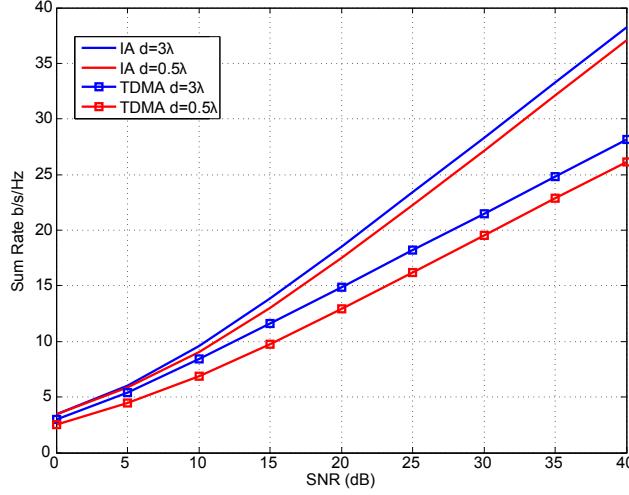


Fig. 9. Network sum rate for IA and TDMA Vs. SNR for the configuration with co-located transmitters for $d = 0.5\lambda$ and $d = 3\lambda$.

be shown to be approximately 1.8 in TDMA and 2.8 for interference alignment, thus confirming the fact that as SNR approaches infinity, interference alignment will provide the maximum achievable degrees of freedom, which in this case is 3.

We note that, at high SNR, there are constant differences between the various measured results in all plots of Figure 7 due, primarily, to varying degrees of spatial correlation and frequency selectivity. Measured results with closely spaced antennas, such as the case where spacing is about 0.5λ , exhibit significantly more spatial correlation across antennas and users, as shown in Figure 6, and thus more aligned channels than the simulated i.i.d. Rayleigh channels. This high correlation decreases SINR after alignment. Varying spatial correlation is also responsible for the constant difference in performance between the different measurement scenarios.

Figure 8 shows that interference alignment benefits from increased antenna and user spacing, with the improvements decreasing with marginal increases of spacing as users become more widely spread. Though the trend in Figure 8, relating the results of Figure 7 and 6 is noticeable, at low levels of correlation this relation is less evident. In fact, SNR after alignment, and thus the performance of IA, is likely to be more tightly related to the distances between the signal subspace, the chosen interference subspace, and the dominant subspace of the user's channel, thus making user spacing and traditional correlation measures only a crude tool for comparison.

In addition to spatial correlation, the simulated i.i.d. Rayleigh channel assumes independent fading on each subcarrier, which corresponds to significantly more frequency selectivity than the levels present in our indoor measurement results. Frequency selectivity is a main factor aiding interference alignment in achieving the maximum number of degrees of freedom, and therefore contributes to the gap between measured and simulated performance [1]. This will be more evident in Section VI, which presents the outdoor measurement results.

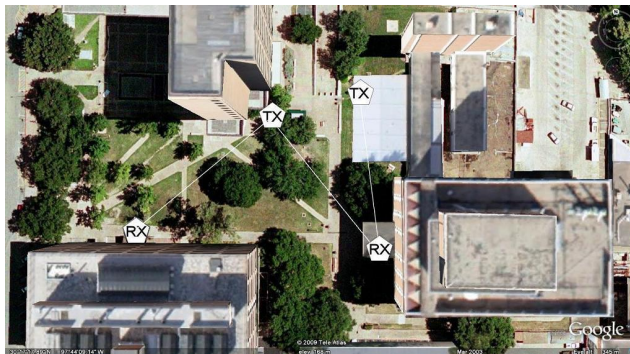


Fig. 10. Area surrounding the Engineering Science Building where the outdoor measurements were taken. The TX/RX hexagons outline the approximate areas in which the 6 transceivers were placed in different configurations and do not imply actual co-location (i.e. antennas were placed around that region with sufficient antenna and user spacing).

In addition to confirming interference alignment's theoretical achievements, our measurements give insight into the effect of node placement on performance, and the feasibility of adopting the iterative algorithms proposed in [5] and [6] in relatively static indoor deployments. Though these algorithms may require thousands of iterations to converge, thus consuming valuable computational power, the static nature of the channels observed suggest that, once found, the precoding matrices can be used over many successive packet transmissions. This fact minimizes the relative overhead incurred by using iterative algorithms.

VI. OUTDOOR RESULTS

We conduct our outdoor experiments in the area surrounding the Engineering Science Building² shown in Figure 10. The environment contains several buildings of steel reinforced concrete, two aluminum annexes, as well as other impeding and reflective objects normally present in a typical outdoor environment. This environment is therefore a good representative medium to study the performance of IA in typical outdoor environments.

Transmitters and receivers are placed approximately 180ft to 200ft apart in both line-of-sight and non-line-of-sight arrangements. To support this long range transmission we use 500mW high gain amplifiers to maintain a receive SNR of 20dB. To verify that the observed channel is in fact a good representative outdoor channel for this study, and thus presents more multipath fading than our previous indoor measurements, Figure 11 shows an example frequency plot the first element of \mathbf{H}_{11} . Figure 11 shows that this outdoor channel is significantly more frequency selective than previous results. Examining the accompanying power delay profile in Figure 12 confirms the presence of 5 channel taps, resulting in a maximum delay spread of 5 sample periods and a

²Picture taken from Google Earth (©2009 Tele Atlas).

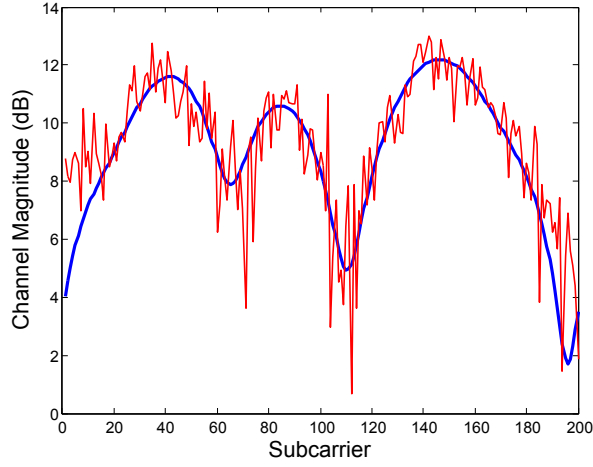


Fig. 11. A sample magnitude plot of \mathbf{H}_{11} in an outdoor NLOS arrangement. This plot shows significantly more selectivity than the channel of 5. The red plot corresponds to the noisy channel estimate, due to low SNR in this case, and the blue plot corresponds to the same channel but includes the effect of only the first 5 channel taps, corresponding to the estimated maximum delay spread, and thus filters out high frequency estimation noise yielding a better “smooth” estimate.

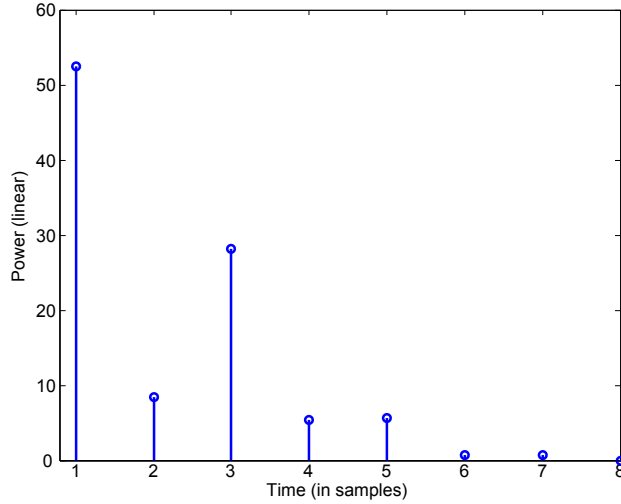


Fig. 12. Power delay profile of the channel shown in 11 showing 5 channel taps. This channel, therefore, has a coherence bandwidth of 3.2 MHz.

channel coherence bandwidth of 3.2 MHz, well under the 16 MHz bandwidth of our signal.

Paralleling the performance analysis done in the indoor case, Figure 13 presents the average achievable sum rate in our outdoor measurements. Figure 13 verifies all claims and conclusions drawn in light of the previous indoor results. We again notice that there are constant differences between the different measurement scenarios in Figure 13. Though the Kronecker model is only a crude tool to study the effect of channel spatial correlation

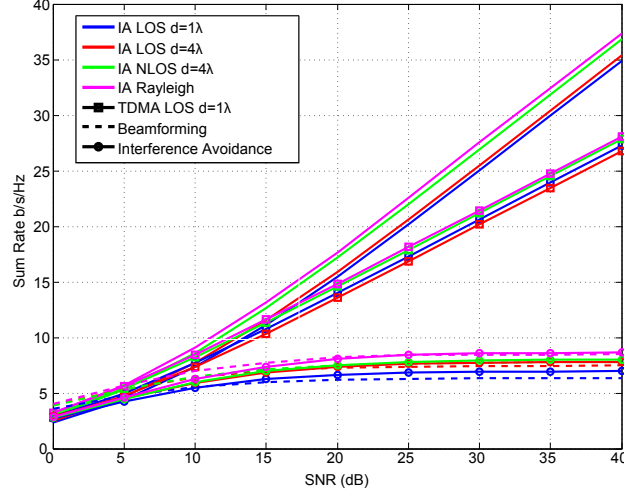


Fig. 13. Network Sum Rate versus SNR for IA, TDMA, SVD Beamforming, and interference avoidance in our outdoor measurement scenarios.

on the performance of IA, the correlation measures are again consistent with the results of Figure 13, and lower correlation yields better sum rates. The NLOS scenarios, showing a receive correlation coefficient of 0.037, performs significantly better than the LOS scenarios with antenna separations of 0.5λ and 4λ , which show receive correlations of 0.1201 and 0.1154 respectively. Also note that in NLOS arrangements, due to an increased reliance on multipath reflections, the channel varies more in space, and thus the channel's spatial correlation across users is lower in this case.

We again show that IA achieves the maximum achievable degrees of freedom in the 3-user interference channel and is thus optimal in the high SNR regime. We also note that IA clearly outperforms orthogonal resource allocation techniques. In addition to outperforming orthogonal techniques such as TDMA, Figure 13 shows that when interference power is equal to the received signal power, IA outperforms SVD transmit beamforming, also known as dominant eigenmode transmission, in which a transmitter, chooses a precoding matrix, or in this case a beamforming vector, to be the channel's dominant eigenvector thus aligning the transmitted signal with the dominant eigenmode of the channel, therefore maximizing SNR at the receiver [24]. Similarly, IA outperforms greedy interference avoidance in which each user k aligns their signals along the whitened channel matrix thus taking into account interference and incrementally improving performance when compared to simple transmit beamforming [25]. Note that this assumes equal received power on all channels. In many realistic ad hoc network deployments, however, communicating nodes are likely to be positioned close to one another, thus receiving different signal and interference powers. This fact makes the comparison of IA, which does not benefit much from decreased interference power, to beamforming, which clearly benefits from lower interference, in a setup where all channel gains are equal, an unfair comparison. For example, at an SIR

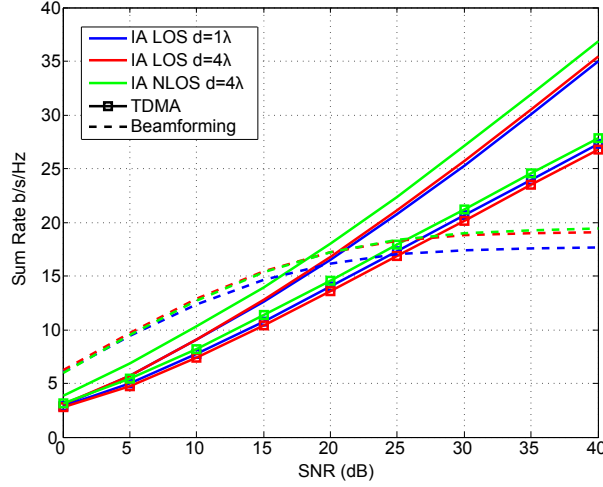


Fig. 14. Achieved sum rate for IA, TDMA and SVD Beamforming when signal is 13dB higher than individual interferers. IA still outperforms all other techniques in the high SNR regime.

level of about 8dB, IA only outperforms interference avoidance at SNR values higher than 20dB, as shown in figure 14. This suggests that depending on the received SIR levels, a network might choose to operate in any of the two transmission schemes. When the network is noise limited at low SNR, interference is insignificant and thus can be avoided, making the greedy beamforming approach superior. As SNR increases, however, the network operates in an interference limited regime where IA clearly dominates. The suboptimality of IA at low to medium SNR also motivates the SINR maximizing algorithm described in sections III-C and shown in Figure 16.

As stated in Section III, the solution to the IA problem is not unique, e.g. in the case of closed form IA, non-uniqueness can be easily seen by changing the order in which we find the precoders \mathbf{F}_l , which results in 3 out of the possibly infinite number of solutions. In iterative IA, and all the other iterative algorithms presented, the non-convexity of the cost function also clearly suggests the existence of local optima and thus the non-uniqueness of the alignment solution. Further, none of the algorithms directly optimize the objective of sum capacity maximization. Therefore, to further increase the achieved sum rate one must select the best performing of the available solution set. In iterative IA, this translates into trying several initializations for the algorithm, and choosing the one that converges to the “best” local optimum, thus providing a higher sum rate. Figure 15 shows that picking the best result out of 10 randomly initialized algorithm outputs yields a constant and non-trivial sum rate increase of about 5b/s/Hz, with different measurement scenarios improving more than others.

Figure 16 plots the sum rates achieved by the iterative SINR maximizing algorithm in selected indoor and

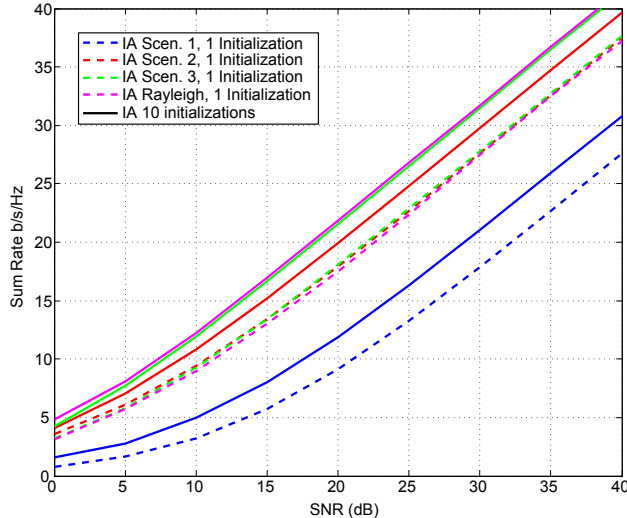


Fig. 15. Iterative IA performance with multiple initializations. Since solutions are not unique, choosing the best from the set of solutions yields a constant increase in sum rate.

outdoor measurement scenarios, and compares them to the sum rates achieved by using IA. As expected, the SINR maximizing algorithm presented outperforms interference alignment, which is oblivious to the resulting SINR within the chosen interference subspace. Also as expected, this performance gap is most noticeable in the low-to-medium SNR regime and decays as we transition to increasingly higher SNR levels at which IA is analytically proven to be optimal in a degrees of freedom sense. Not only do the benefits of using the SINR maximizing algorithm decrease at high SNR, the cost of this algorithm in this regime increases as well. Figure 17 clearly shows the increasing number of iterations needed for MAX SINR to start outperforming closed form IA. The same thing can be said about the absolute convergence of the MAX SINR algorithm: as SNR increases, the number of iterations needed for convergence increases.

VII. PRACTICAL IMPERFECTIONS

The results presented thus far, coupled with the heavy reliance on network-wide channel state information, suggest that IA's claimed performance, though achievable may suffer sum rate losses in real systems not satisfying IA's ideal demands. Consequently, in this section, we provide results based on measurement and simulation to characterize the adverse effect channel and system imperfections may have on IA.

We first address a subtle practical concern when evaluating IA over real wireless links: the effect of channel estimation and feedback delay. IA, as shown in III requires full channel state information, either to be fed back to the transmitter, or to calculate the precoders at the receiver which in turn are fed back. Therefore, unlike TDMA, for example, which has minimal use for channel estimates, IA relies heavily on the channel estimates

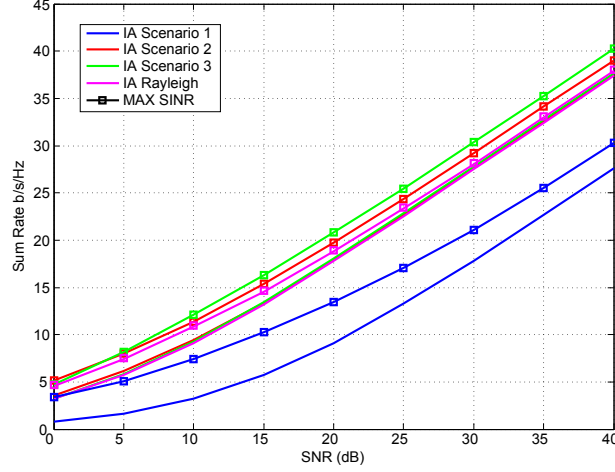


Fig. 16. Sum rate Vs. SNR plots for interference alignment and the MAX SINR Algorithm. While both algorithms converge at high SNR, MAX SINR outperforms IA at low SNR when noise is a significant limiting factor in the network.

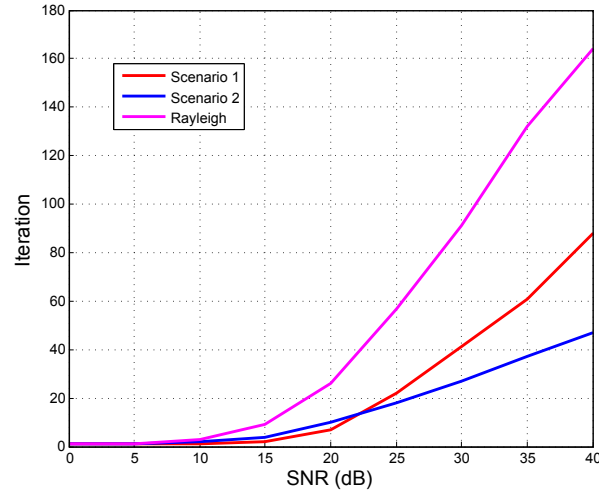


Fig. 17. Number of iterations needed for MAX SINR to outperform IA. As SNR increases, not only does MAX SINR lose its advantage over IA, but the number of iterations the algorithm takes to outperforms closed form IA also increases superlinearly.

over all links. Figure 18 shows the performance of a MIMO-OFDM IA system over an average of measured and simulated Rayleigh channel. We consider channel estimates that have been corrupted by i.i.d. zero mean Gaussian noise.

For a fixed channel gain, of squared Frobenius norm of 4, we plot the performance of the system for various norms of the estimate error matrix. Figure 18 shows that channel estimation error has a saturating effect on IA performance. This observation contributes to the practical suboptimality of IA in the low SNR regime where

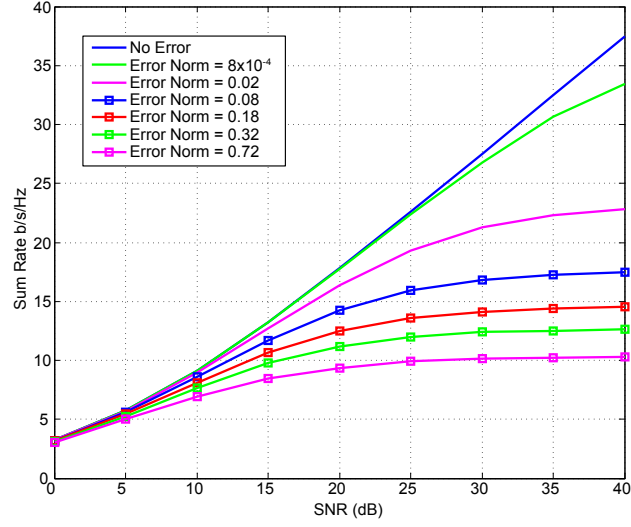


Fig. 18. IA performance with channel estimation error. The use of imperfect CSI diminishes the gains of using IA and saturates the achievable rate at high SNR.

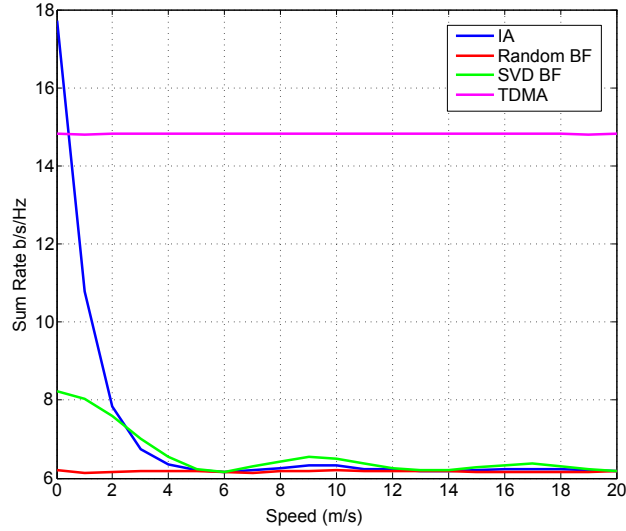


Fig. 19. The effect of feedback delay on the performance of IA ($SNR = 40dB$). With delayed feedback, the CSI used is outdated, which results in the wrong choice of precoders and thus reduced sum rate. In fact, at a speed of just 4m/s, with feedback delay of 10ms, IA performs within one bit of random beamforming.

channel estimates are likely to be noisy, and may also effect OFDM systems using per-tone frequency domain channel estimation even at high SNR.

Figure 19 in turn shows the effect of feedback delay on the performance of IA in a time varying channel. We plot, for varying mobile station speed, the sum rate achieved by an IA system at 2.4 GHz, with a feedback

delay of 10ms. For this plot we assume that the normalized delayed channel data, \mathbf{H}_{t-1} , is perfectly known and is generated according to a simple first order fading model

$$\mathbf{H}_t = \alpha \mathbf{H}_{t-1} + \bar{\alpha} \mathbf{N}_t, \quad (19)$$

where \mathbf{H}_t is the channel at time t , \mathbf{N}_t is a 2×2 i.i.d. complex Gaussian matrix with elements of unit variance, $\bar{\alpha} = \sqrt{1 - \alpha^2}$ and α is a correlation coefficient given by

$$\alpha = J_0 \left(\frac{2\pi T v}{\lambda} \right), \quad (20)$$

where T is the feedback delay, and v is the speed of mobile station moving in random directions. As illustrated in Figure 19, the performance of IA with delayed, and thus imperfect, CSI drops rapidly with motion. In fact nodes moving at only 2m/s will suffer a 11 bit loss, and at increasingly high Doppler, the performance of IA converges to the performance of random beamforming since the delayed channel information and the actual observed channel become “increasingly independent”. Additional simulation shows that the use of multiple random initializations, while beneficial in the case of perfect channel knowledge does not improve performance with imperfect CSI. Therefore, while iterative algorithms can be used in networks with statically positioned nodes, and thus channels with slow temporal evolution, feedback delay and convergence time, if not treated, will have an adverse effect on IA’s performance.

While we can partially attribute estimation error and feedback delay to imperfections in practically implemented systems, pure realistic channel imperfections also affect IA in practice. In Section V we showed that channel spatial correlation may affect IA performance negatively. In that section, however, we examined only correlation across a user’s antenna using simple Kronecker correlation. While a general trend of increasing performance with lower correlation was observed, this is common to most MIMO techniques. IA, however, in addition to being affected by the condition of each user’s channel also relies on cross channels for alignment. Therefore, correlation across users is likely to affect IA’s performance. To illustrate this point, we study the effect channel matrix collinearity, another typical correlation measure considered in practice [37], has on the performance IA. The collinearity between two matrices \mathbf{A} and \mathbf{B} is defined as [38]

$$c(\mathbf{A}, \mathbf{B}) = \frac{|\text{trace}(\mathbf{A}\mathbf{B}^*)|}{\|\mathbf{A}\|_F \|\mathbf{B}\|_F} \quad (21)$$

Figure 20 shows that while the average collinearity of a channel matrices in the network increases, IA’s performance monotonically decreases. Matrix collinearity, therefore, is more closely related to IA’s performance than correlation in the Kronecker model sense. This is not without reason, as we stated in V, the factor directly controlling the achieved sum rate is SNR after alignment, which is directly related to the relative distance between the chosen signal and interference subspaces. While this definition of collinearity is affected by the

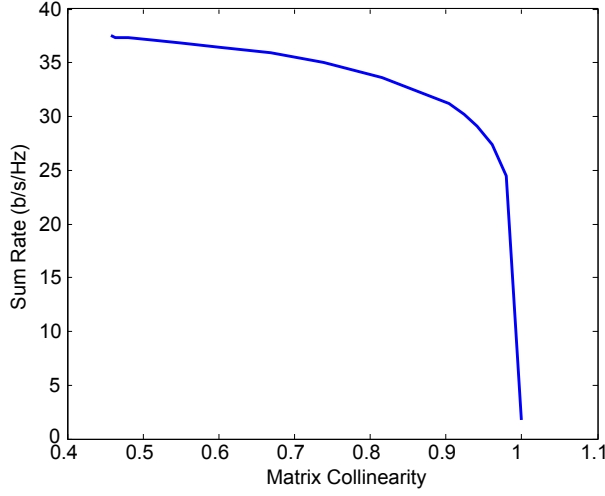


Fig. 20. The effect of channel collinearity on IA performance ($SNR = 40dB$). As collinearity increases, column spaces are more aligned, which in turn reduces SNR after alignment.

ordering of the columns of \mathbf{A} and \mathbf{A} , it is mainly a measure of the similarity of the subspaces spanned by the channel matrices in the network. High collinearity translates into highly aligned signal subspaces and, consequently, lower SNR after alignment. To better illustrate this, examining equations (9), (10), and (11) and considering the worst case of perfectly aligned channels in the network, we can see that the chosen precoders are all related by at most a rotation, and thus all lie in the same subspace. When used across these perfectly aligned channels, these precoders result in perfectly aligned signal and interference effective channels, $\mathbf{H}_{k,k}\mathbf{F}_k$ and $\mathbf{H}_{k,m}\mathbf{F}_m$, drastically decreasing the achieved sum rate.

While matrix collinearity provides an intuitive correlation measure that can be linked to the performance of IA through the monotonic relation shown in Figure 20, the sum rate achieved is more tightly linked to the SNR after projection onto the interference free space. Therefore, sum rate can be directly linked to the distance between the subspaces spanned by the effective channel $\mathbf{H}_{km}\mathbf{F}_m$, which collinearity does not directly measure; collinearity, though considered in practice, is affected by the ordering of the basis vectors and is thus not a perfect measure for subspace distance. To illustrate this, we first define the projection F-norm distance [39] between two subspaces with orthonormal basis \mathbf{U} and \mathbf{V} as

$$d_{pF}(\mathbf{U}, \mathbf{V}) = \frac{1}{\sqrt{2}} \|\mathbf{U}\mathbf{U}^* - \mathbf{V}\mathbf{V}^*\|_F. \quad (22)$$

To incorporate the distances between all channels, as well as signal and interference subspaces present in the network, we define two projection F-norm based distances, namely the average subspace distance between the

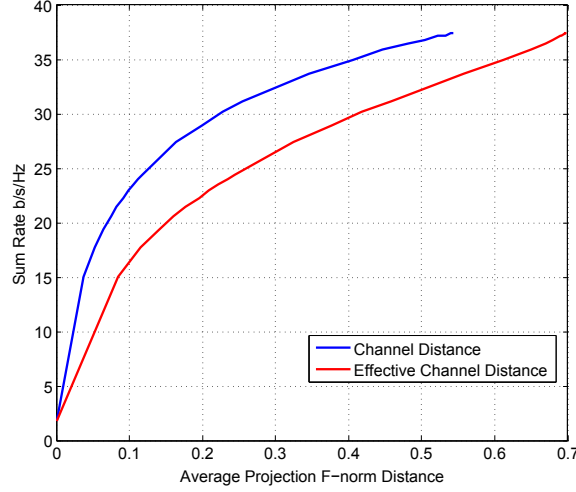


Fig. 21. The effect of the average distance defined in equation (23) on IA performance. As the subspaces spanned by the effective channels grow farther apart, SNR after alignment and, consequently, sum rate increases.

set of effective channels $\mathbf{H}_{km}\mathbf{F}_m$ as

$$d(\{\mathbf{H}\mathbf{F}\}) = \sqrt{\frac{\sum_{k,m \in \{1,2,3\}} d_{pF}(\Psi(\mathbf{H}_{kk}\mathbf{F}_k), \Psi(\mathbf{H}_{km}\mathbf{F}_m))^2}{\binom{K}{K-1}}}, \quad (23)$$

and the average column space distance between the set of channels \mathbf{H}_{km}

$$d(\{\mathbf{H}\}) = \sqrt{\frac{\sum_{k,m \in \{1,2,3\}} d_{pF}(\Psi(\mathbf{H}_{kk}), \Psi(\mathbf{H}_{km}))^2}{\binom{K}{K-1}}}, \quad (24)$$

where $\Psi(\mathbf{A})$ is the operator that extracts the orthonormal basis for the column space of \mathbf{A} . In the special case of equation (23), where $\mathbf{H}_{km}\mathbf{F}_m$ are vectors, $\Psi(\mathbf{H}_{km}\mathbf{F}_m)$ simply returns the normalized vector spanning that space.

Having defined these distance metrics, Figure 21 plots the sum rate achieved by interference alignment at SNR= 40dB vs. the distances defined in equations (23) and (24). We see that as the subspaces spanned by the signal and interference effective channels become farther apart, IA's performance monotonically increases. The reason for this is that after choosing an interference free space, i.e. a space orthogonal to the received interference, the linear IA decoder projects onto the basis of that space to decode. Hence, the more aligned the signal and interference spaces are, the smaller the signal component in the interference free subspace will be, thus, diminishing both post-projection SNR and the achieved sum rate. Moreover, the similar monotonic relationship linking the sum rate performance to the distance between the column spaces of the channels

themselves, confirms the intuition that closer aligned channels result in closer aligned signal and interference subspaces.

VIII. CONCLUSION AND FUTURE WORK

In this paper, we have presented the first MIMO interference channel testbed programmed using a flexible software defined radio base. We have presented indoor and outdoor network channel measurements collected in our university environment, and then processed them to evaluate the performance gains of IA in such node deployments. We showed that the observed gains closely parallel those found through theory and simulation. In subsequent work we will extend the measurement setup beyond three users as well close the feedback loop in order to implement a real time closed loop IA system. This effort will be a major step in transforming interference alignment from a theoretical algorithm for the simple interference channel, to large scale interference limited mobile ad hoc networks.

REFERENCES

- [1] V. Cadambe and S. Jafar, "Interference alignment and degrees of freedom of the K-user interference channel," *IEEE Transactions on Information Theory*, vol. 54, no. 8, pp. 3425–3441, August 2008.
- [2] M. Maddah-Ali, A. Motahari, and A. Khandani, "Signaling over MIMO multi-base systems: combination of multi-access and broadcast schemes," *Proc. of IEEE International Symposium on Information Theory*, pp. 2104–2108, July 2006.
- [3] S. Jafar and M. Fakhreddin, "Degrees of freedom for the MIMO interference channel," *Proc. of IEEE International Symposium on Information Theory*, pp. 1452–1456, July 2006.
- [4] S. Jafar and S. Shamai, "Degrees of freedom region of the MIMO X channel," *IEEE Transactions on Information Theory*, vol. 54, no. 1, pp. 151–170, January 2008.
- [5] K. Gomadam, V. Cadambe, and S. Jafar, "Approaching the capacity of wireless networks through distributed interference alignment," *Proc. of IEEE Global Telecommunications Conference*, pp. 1–6, December 2008.
- [6] S. W. Peters and R. W. Heath, Jr., "Interference alignment via alternating minimization," *Proc. of IEEE International Conference on Acoustics, Speech, and Signal Processing*, April 2009.
- [7] R. Tresch, M. Guillaud, and E. Riegler, "On the achievability of interference alignment in the K-User constant MIMO interference channel," *Proc. of IEEE Workshop on Statistical Signal Processing*, pp. 277–280, September 2009.
- [8] C. Suh and D. Tse, "Interference alignment for cellular networks," *Proc. of Allerton Conference on Communication, Control, and Computing*, pp. 1037–1044, September 2008.
- [9] S. W. Choi, S. A. Jafar, and S. Chung, "On the Beamforming Design for Efficient Interference Alignment," *ArXiv e-prints*, June 2009.
- [10] I. Thukral and H. Bolcskei, "Interference alignment with limited feedback," *Proc. of IEEE International Symposium on Information Theory*, pp. 1759–1763, July 2009.
- [11] C. M. Yetis, S. A. Jafar, and A. H. Kayran, "Feasibility conditions for interference alignment," *CoRR*, vol. abs/0904.4526, 2009.
- [12] C. Huang, S. A. Jafar, S. Shamai, and S. Vishwanath, "On degrees of freedom region of MIMO networks without CSIT," 2009. [Online]. Available: <http://www.citebase.org/abstract?id=oai:arXiv.org:0909.4017>
- [13] R. Tresch and M. Guillaud, "Cellular interference alignment with imperfect channel knowledge," *IEEE International Conference on Communications (ICC), Workshop on LTE Evolution, Dresden, Germany*, June 2009.
- [14] O. Johnson, M. Aldridge, and R. Piechocki, "Interference alignment-based sum capacity bounds for random dense gaussian interference networks," 2009. [Online]. Available: <http://www.citebase.org/abstract?id=oai:arXiv.org:0907.5165>

- [15] J. Koivunen, P. Almers, V.-M. Kolmonen, J. Salmi, A. Richter, F. Tufvesson, P. Suvikunnas, A. Molisch, and P. Vainikainen, "Dynamic multi-link indoor MIMO measurements at 5.3GHz," *Proc. of European Conference on Antennas and Propagation*, pp. 1–6, November 2007.
- [16] F. Kaltenberger, M. Kountouris, D. Gesbert, and R. Knopp, "On the tradeoff between feedback and capacity in measured MU-MIMO channels," *IEEE Transactions on Wireless Communications*, vol. 8, no. 9, pp. 4866–4875, September 2009.
- [17] G. Bauch, J. Bach Andersen, C. Guthy, M. Herdin, J. Nielsen, J. Nossek, P. Tejera, and W. Utschick, "Multiuser MIMO channel measurements and performance in a large office environment," *Proc. of IEEE Wireless Communications and Networking Conference*, pp. 1900–1905, March 2007.
- [18] S. Gollakota, S. D. Perli, and D. Katabi, "Interference alignment and cancellation," *SIGCOMM Computer Communication Review*, vol. 39, no. 4, pp. 159–170, 2009.
- [19] O. El Ayach, S. W. Peters, and R. W. Heath, Jr., "Real world feasibility of interference alignment using MIMO-OFDM channel measurements," *Proc. of IEEE Conference on Military Communications*, October 2009.
- [20] G. Stuber, J. Barry, S. McLaughlin, Y. Li, M. Ingram, and T. Pratt, "Broadband MIMO-OFDM wireless communications," *Proceedings of the IEEE*, vol. 92, no. 2, pp. 271–294, Feb 2004.
- [21] A. van Zelst and T. Schenk, "Implementation of a MIMO OFDM-based wireless lan system," *IEEE Transactions on Signal Processing*, vol. 52, no. 2, pp. 483–494, Feb. 2004.
- [22] H. Bolcskei, D. Gesbert, and A. Paulraj, "On the capacity of wireless systems employing OFDM-based spatial multiplexing," *IEEE Transactions on Communication*, vol. 50, pp. 225–234, February 2002.
- [23] S. W. Peters and R. W. Heath, Jr., "Cooperative algorithms for the MIMO interference channel," *submitted*, November 2009.
- [24] A. Paulraj, R. Nabar, and D. Gore, *Introduction to Space-Time Wireless Communications*. New York, NY, USA: Cambridge University Press, 2008.
- [25] C. Rose, S. Ulukus, and R. Yates, "Wireless systems and interference avoidance," *IEEE Transactions on Wireless Communications*, vol. 1, pp. 415–428, July 2002.
- [26] S. Ye and R. Blum, "Optimized signaling for MIMO interference systems with feedback," *IEEE Transactions on Signal Processing*, vol. 51, no. 11, pp. 2839–2848, Nov 2003.
- [27] I. Barhumi, G. Leus, and M. Moonen, "Optimal training design for MIMO OFDM systems in mobile wireless channels," *IEEE Transactions on Signal Processing*, vol. 51, no. 6, pp. 1615–1624, 2003.
- [28] Q. Rahman and M. Hefnawi, "Channel estimation methods for MIMO-OFDM system: time domain versus frequency domain," *Proc. of Canadian Conference on Electrical and Computer Engineering*, vol. 2, pp. 689–692 Vol.2, May 2004.
- [29] E. Zhou, X. Zhang, H. Zhao, and W. Wang, "Synchronization algorithms for MIMO OFDM systems," *Proc. of IEEE Wireless Communications and Networking Conference*, vol. 1, pp. 18–22 Vol. 1, March 2005.
- [30] National Instruments, "NI PXI-1045 Data Sheet," 2009. [Online]. Available: <http://www.ni.com/pdf/products/us/pxi1045.pdf>
- [31] —, "NI PXI-5670 Data Sheet," 2009. [Online]. Available: http://www.ni.com/pdf/products/us/5670_datasheet.pdf
- [32] —, "NI PXI-5660 Data Sheet," 2009. [Online]. Available: <http://www.ni.com/pdf/products/us/4mi469-471.pdf>
- [33] A. Gupta, A. Forenza, and R. W. Heath, Jr., "Rapid MIMO-OFDM software defined radio system prototyping," *Proc. of IEEE Workshop on Signal Processing Systems*, October 2004.
- [34] National Instruments, "NI PXI-6653 Data Sheet." [Online]. Available: http://www.ni.com/pdf/products/us/pxi665x_pxie6672_datasheet.pdf
- [35] C. A. Balanis, *Antenna Theory: Analysis and Design*. New York, NY: Wiley, 1997.
- [36] J. Wallace, M. Jensen, A. Swindlehurst, and B. Jeffs, "Experimental characterization of the MIMO wireless channel: Data acquisition and analysis," *IEEE Transactions on Wireless Communications*, vol. 2, no. 2, pp. 335–343, 2003.
- [37] N. Czink, B. Bandemer, G. Vilar, L. Jalloul, and A. Paulraj, "Can multi-user MIMO measurements be done using a single channel sounder?" *COST 2100, TD (08), Lille, France, October 2008*, vol. 621.
- [38] G. Golub and C. Van Loan, *Matrix computations*. Johns Hopkins Univ Pr, 1996.

- [39] A. Edelman, T. A. Arias, and S. T. Smith, “The geometry of algorithms with orthogonality constraints,” *SIAM Journal on Matrix Analysis and Applications*, vol. 20, no. 2, pp. 303–353, 1998.